

The Hubbard model with intersite interaction within the Composite Operator Method

Adolfo Avella* and Ferdinando Mancini†

*Dipartimento di Fisica “E.R. Caianiello” - Unità di Ricerca INFN di Salerno
Università degli Studi di Salerno, I-84081 Baroness (SA), Italy*

(Dated: March 22, 2022)

We study the one- and two- dimensional extended Hubbard model by means of the Composite Operator Method within the 2-pole approximation. The fermionic propagator is computed fully self-consistently as a function of temperature, filling and Coulomb interactions. The behaviors of the chemical potential (global indicator) and of the double occupancy and nearest-neighbor density-density correlator (local indicators) are analyzed in detail as primary sources of information regarding the instability of the paramagnetic (metal and insulator) phase towards charge ordering driven by the intersite Coulomb interaction. Very rich phase diagrams (multiple first and second order phase transitions, critical points, reentrant behavior) have been found and discussed with respect to both metal-insulator and charge ordering transitions: the connections with the experimental findings relative to some manganese compounds are analyzed. Moreover, the possibility of improving the capability of describing cuprates with respect to the simple Hubbard model is discussed through the analysis of the Fermi surface and density of states features. We also report about the specific heat behavior in presence of the intersite interaction and the appearance of crossing points.

I. INTRODUCTION

Many authors have emphasized the importance of considering non-local Coulomb interactions in describing doped systems like cuprate superconductors or fullerides^{1,2,3,4,5}. The simplest Hamiltonian satisfying these requirements is the extended Hubbard model, where a nearest-neighbor Coulomb interaction term is added to the original Hubbard Hamiltonian⁶. The inclusion of non-local Coulomb interactions substantially modifies the electronic properties of the model. For instance, the charge transfer excitons, which can only be detected by optical spectroscopy at half filling, attain some charge in doped systems and become visible in direct and inverse photoelectron spectroscopies⁷. Other studies, using an effective extended Hubbard model, support the appearance, upon doping, of states evenly distributed inside the gap⁸. This suggests that the general features of the cuprates can be well described by using this effective Hubbard Hamiltonian, which has also been used to mimic some of their experimental features in the superconducting state by means of a BCS treatment⁹.

The Hubbard model with intersite Coulomb interaction is also one of the simplest models capable to describe charge ordering (CO) in interacting electron systems. Already in 1938 Wigner proposed¹⁰ that a low density interacting electron gas crystallizes in a lattice in order to minimize the Coulomb repulsion. At higher densities crystallization is possible if the kinetics energy is reduced by spin or phonon interactions¹¹. Charge ordering has been experimentally observed in a variety of systems: *GaAs/AlGaAs* heterostructures¹², rare-earth pnictides like *Yb₄As₃*¹³, colossal magnetoresistance compounds¹⁴, unconventional spin-Peierls materials α -*NaV₂O₅*¹⁵, cuprates¹⁶, manganites¹⁷, magnetite¹⁸, vanadium oxides¹⁹, Bechgaard salts²⁰.

Among the many analytical methods used to study

the extended Hubbard model we recall: Hartree-Fock approximation²¹, perturbation theory²², dynamical mean field theory²³, slave boson approach^{24,25}, coherent potential approximation²⁶. Numerical studies by means of Quantum Monte Carlo²⁷, Lanczos technique²⁸ and exact diagonalization²⁹ have also to be recalled.

In this manuscript, we analyze the extended Hubbard model by means of the Composite Operator Method (COM) within the 2-pole approximation (see Refs. 30,31 and references therein).

The COM is based on two main concepts: (i) the excitations present in interacting systems are far from being the original electrons and need to be described by asymptotic fields in the form of composite operators; (ii) the use of composite operators requires the enforcement of the non-canonical algebra they obey in order to properly fix the representation where their propagators are realized. This latter task is effectively undertaken by computing the values of the unknown correlators appearing in the calculations by means of Algebra Constraints³⁰.

The detailed analysis of the instabilities of the homogenous paramagnetic phase of the extended Hubbard model towards charge ordered inhomogeneous phases is the main task undertaken with this manuscript. With respect to this, we have analyzed the rank of the transitions and their relations with the metal-insulator one. Actually, this study is the only relevant at room temperatures and/or in presence of frustration as any spin ordered phase (e.g., the antiferromagnetic phase) would be inaccessible in such situations. It is worth noticing that the very rich phase diagrams (multiple first and second order phase transitions, critical points, reentrant behavior) that have been found can be put in connection with the experimental findings relative to some manganese compounds^{32,33,34}. We have also discussed in detail the possibility of improving the capability of describing cuprates with respect to the simple Hubbard model

and the appearance of crossing points in the specific heat in presence of the intersite interaction.

In the next section we present the model, the basis and the solution according to the COM. In the subsequent sections, we comment our results for the chemical potential, the phase diagram, the double occupancy, the nearest-neighbor density-density correlator, the internal and kinetic energies, the Fermi surface, the density of states and the specific heat. The types of charge ordered phases found according to the sign of the intersite potential are described, the rank of the transitions is evidenced through the analysis of the discontinuities in the chemical potential, double occupancy, nearest-neighbor density-density correlator and kinetic and internal energies, quite complex phase diagram (with metal to insulator and to charge ordered phase transitions and reentrant behavior) are drawn and commented, the behavior of single- (double occupancy) and two- (nearest-neighbor charge) site correlators is studied in order to get information about the actual charge distribution, the value of the filling at which the nesting appear is determined as a function of intersite potential, the specific heat behavior is studied in comparison to that of the simple Hubbard model.

II. HAMILTONIAN, FIELD EQUATIONS AND SOLUTION

We will study a generalized version of the Hubbard model⁶ which includes the intersite Coulomb interaction^{35,36,37,38,39,40,41}. Accordingly, the Hamiltonian under analysis reads as

$$H = \sum_{\mathbf{i}} [-\mu c^\dagger(\mathbf{i})c(\mathbf{i}) - 2dt c^\dagger(\mathbf{i})c^\alpha(\mathbf{i})] + \sum_{\mathbf{i}} [Un_\uparrow(\mathbf{i})n_\downarrow(\mathbf{i}) + dVn(\mathbf{i})n^\alpha(\mathbf{i})] \quad (2.1)$$

where μ is the chemical potential, $c^\dagger(\mathbf{i}) = (c^\dagger_\uparrow(\mathbf{i})c^\dagger_\downarrow(\mathbf{i}))$ is the creation electronic operator in spinorial notation, $\mathbf{i} = (\mathbf{i}, t)$, \mathbf{i} is one lattice vector of the d -dimensional square lattice, t , as usually done in the related literature, is both the time variable and the hopping integral, the context will clarify the use, U is the onsite Coulomb interaction, V is the intersite interaction, $n(\mathbf{i}) = n_\uparrow(\mathbf{i}) + n_\downarrow(\mathbf{i})$, $n_\sigma(\mathbf{i})$ is the number operator for electrons of spin σ . Hereafter, t will be used as reference unit for all energies. We have used the notation

$$\phi^\alpha(\mathbf{i}, t) = \sum_{\mathbf{j}} \alpha_{\mathbf{ij}} \phi(\mathbf{j}, t) \quad (2.2)$$

where ϕ can be any operator and $\alpha_{\mathbf{ij}}$ is the projector on the first $2d$ neighbor sites on the lattice. We have $\alpha(\mathbf{k}) = \mathcal{F}[\alpha_{\mathbf{ij}}] = 1/d \sum_{n=1}^d \cos(k_n)$, where \mathcal{F} is the Fourier transform.

Within the Composite Operator Method³⁰, once we choose a n -component spinorial basis $\psi(\mathbf{i})$, the equations

of motion of this latter take the general form

$$i \frac{\partial}{\partial t} \psi(\mathbf{i}, t) = \sum_{\mathbf{j}} \epsilon(\mathbf{i}, \mathbf{j}) \psi(\mathbf{j}, t) + \delta j(\mathbf{i}, t) \quad (2.3)$$

where $\epsilon(\mathbf{k}) = \mathcal{F}[\epsilon(\mathbf{i}, \mathbf{j})]$ is the $n \times n$ energy matrix describing the projected dynamics. The energy matrix can be computed as $\epsilon(\mathbf{k}) = m(\mathbf{k})I^{-1}(\mathbf{k})$ where $I(\mathbf{k}) = \mathcal{F}\{\langle \psi(\mathbf{i}, t), \psi^\dagger(\mathbf{j}, t) \rangle\}$ is the normalization matrix of the basis and $m(\mathbf{k}) = \mathcal{F}\{\langle i \frac{\partial}{\partial t} \psi(\mathbf{i}, t), \psi^\dagger(\mathbf{j}, t) \rangle\}$. If we neglect $\delta j(\mathbf{i})$ we obtain a pole structure for the retarded thermal Green's function $G(\mathbf{k}, \omega) = \mathcal{F}\langle \mathcal{R}[\psi(\mathbf{i})\psi^\dagger(\mathbf{j})] \rangle$ (\mathcal{R} is the retarded operator) that will obey the following equation of motion

$$\omega G(\mathbf{k}, \omega) = I(\mathbf{k}) + \epsilon(\mathbf{k})G(\mathbf{k}, \omega) \quad (2.4)$$

The solution of Eq. (2.4) is

$$G(\omega, \mathbf{k}) = \sum_{i=1}^n \frac{\sigma^{(i)}(\mathbf{k})}{\omega - E_i(\mathbf{k}) + i\delta} \quad (2.5)$$

where $E_i(\mathbf{k})$ are the eigenvalues of $\epsilon(\mathbf{k})$ and the spectral weights $\sigma^{(i)}(\mathbf{k})$ can be computed as

$$\sigma_{ab}^{(i)}(\mathbf{k}) = \sum_{c=1}^n \Omega_{ai}(\mathbf{k}) \Omega_{ic}^{-1}(\mathbf{k}) I_{cb}(\mathbf{k}) \quad a, b = 1, \dots, n \quad (2.6)$$

where the matrix $\Omega(\mathbf{k})$ has the eigenvectors of $\epsilon(\mathbf{k})$ as columns³⁰. In this manuscript, we will use a 2-pole approximation within the COM. The reader interested to more elaborate self-energy treatments (in order to take into account $\delta j(\mathbf{i})$ we should compute the higher order propagator $\langle \mathcal{R}[\delta j(\mathbf{i})\delta j^\dagger(\mathbf{j})] \rangle$) should refer, for instance, to Ref. 42,43,44.

For the model under analysis in this manuscript, we choose, as basic fields, the Hubbard operators, which faithfully describe the Hubbard subbands as eigenoperators of the ionic model,

$$\psi(\mathbf{i}) = \begin{pmatrix} \xi(\mathbf{i}) \\ \eta(\mathbf{i}) \end{pmatrix} \quad (2.7)$$

where $\xi(\mathbf{i}) = n(\mathbf{i})c(\mathbf{i})$ and $\eta(\mathbf{i}) = c(\mathbf{i}) - \xi(\mathbf{i}) = [1 - n(\mathbf{i})]c(\mathbf{i})$. They satisfy the following equations of motion

$$i \frac{\partial}{\partial t} \psi(\mathbf{i}) = \begin{pmatrix} -\mu \xi(\mathbf{i}) - 2d[tc^\alpha(\mathbf{i}) + t\pi(\mathbf{i}) - V\xi(\mathbf{i})n^\alpha(\mathbf{i})] \\ -(\mu - U)\eta(\mathbf{i}) + 2d[t\pi(\mathbf{i}) + V\eta(\mathbf{i})n^\alpha(\mathbf{i})] \end{pmatrix} \quad (2.8)$$

where

$$\pi(\mathbf{i}) = \frac{1}{2} \sigma^\mu n_\mu(\mathbf{i}) c^\alpha(\mathbf{i}) + c(\mathbf{i}) c^{\alpha\dagger}(\mathbf{i}) c(\mathbf{i}) \quad (2.9)$$

$\sigma^\mu = (-1, \vec{\sigma})$, $n_\mu(\mathbf{i}) = (n(\mathbf{i}), \vec{n}(\mathbf{i}))$ is the charge and spin number operator, $\vec{n}(\mathbf{i}) = c^\dagger(\mathbf{i}) \vec{\sigma} c(\mathbf{i})$ and $\vec{\sigma}$ are the Pauli matrices.

After the choice we made for the basis, we can compute, in the 2-pole approximation within COM, the energy spectra $E_i(\mathbf{k})$ and the spectral density functions $\sigma^{(i)}(\mathbf{k})$ according to the general procedure given above. The lengthy expressions can be found in Appendix. It is worth noting that some parameters, not connected to the Green's function under analysis, appear in the expressions: $\chi_c^\alpha = \langle n(i)n^\alpha(i) \rangle$ and $p = \frac{1}{4}\langle n_\mu^\alpha(i)n_\mu(i) \rangle - \langle [c_\uparrow(i)c_\downarrow(i)]^\alpha c_\downarrow^\dagger(i)c_\uparrow^\dagger(i) \rangle$. The first one, χ_c^α , will be computed by calculating the density-density correlation function $\langle n(i)n(j) \rangle$ within the one-loop approximation⁴⁵ (see second equation in Eqs. (A10)). The second will be fixed by the local algebra constraint³⁰ $\langle \xi(i)\eta^\dagger(i) \rangle = 0$. Such a procedure is very peculiar to the COM treatment³⁰ as discussed in the introduction. By solving the set of coupled self-consistent equations (A9-A10), we can calculate the various correlation functions and the physical properties of the system. Results will be presented in the following sections for the one-dimensional (1D) and the two-dimensional (2D) systems.

Before moving to the results, it is worth noting that the set of self-consistent equations (A9-A10) is highly non-linear. According to this, it is natural to expect a certain number of coexisting solutions with quite different features. Actually, the set admits only two distinct solutions that, hereafter, we will call COM1 and COM2, according to the main sign of parameter p . In particular, as a function of the filling, we have a p positive and of the order of the filling in COM1 and a p negative or very small and positive in COM2. As the Composite Operator Method tries to give answers in the whole space of model and physical parameters and as the Hubbard model response is profoundly different according to the region of the latter space, the presence of two solutions, so different in their features, should be seen as a richness of the method. Due to the difficulties inherent to the task of studying the whole phase diagram, many other approximations focus just on one region and usually give wrong results in the rest of the parameter space. COM, also thanks to the opportunity of choosing between the two solutions according to the features one expects to describe, has proved to be capable to explore the whole phase diagram, to get significantly good results for all dimensions and values of the tuning parameters, to give relevant interpretations of the experimental facts and to constitute a solid basis for further investigations. It is also worth remembering that, at the end of the day, our analysis has, as main goal, the description of features, more or less anomalous, of real physical systems by means of Hamiltonian models. We can never be sure that our Hamiltonian contains all, and only, relevant ingredients. Different experimental situations can be described by different analytical (and/or numerical) solutions of the same Hamiltonian. For a fixed set of parameters (filling, temperature, pressure, ...), the different solutions will have different free energies and one can simply think to choose one or the other according to this. This is the correct procedure if we wish to answer

the question: "Which is the phase effectively described by this Hamiltonian under such external conditions?". On the other hand, a solution different from the one with lower free energy can better describe the real experimental situation. This latter, although mainly determined by the ingredients already present in the Hamiltonian (the possibility to find a solution with similar characteristics assures this), is that effectively realized in nature owing to some marginal interactions not present in the Hamiltonian chosen. If we would include such interactions in the Hamiltonian and compute new solutions, we will find that the lower free energy one will be the one capable to describe the actual physical situation. Now, the most important consideration to be done is that this latter solution will be essential identical to that obtained with the previous Hamiltonian and that was already capable to describe the actual physical situation although it has not the lower free energy. According to this, in the comparison with the experiments no solution can be discarded a priori (neither on the basis of the free energy determination) and, with this idea in mind, we have here, and in many other works, presented the results for the two solutions we have obtained.

For the one-dimensional system we will consider only COM2 solution as our past experience suggests that this is the one best suited to describe the physics of the simple one-dimensional Hubbard model for which we got excellent agreements with the Bethe Ansatz exact solution^{46,47,48,49}. For the two-dimensional case, we will study both solutions as they will permit us to analyze, in particular in proximity of half filling and as regards the metal-insulator transition and its relation to the charge ordering transition, two different behaviors that could be both observed experimentally. Also in this case the many positive comparisons with numerical results, that we have obtained in the previous studies on the simple two-dimensional Hubbard model^{45,50,51,52,53,54}, will be used as a guide throughout all the analysis.

III. THE CHEMICAL POTENTIAL

The chemical potential can be determined as a function of the parameters n , T , U , V by solving the system of self-consistent equations (A9-A10). It is worth noticing that our results show that the relation

$$\mu(2 - n) = U + 4dV - \mu(n) \quad (3.1)$$

required by the particle-hole symmetry, is exactly satisfied. In particular at half filling we have $\mu(1) = \frac{1}{2}U + 2dV$. This is due to the fact that among the possible representations the Algebra Constraint coming from the Pauli principle [see first equation in Eqs. (A10)] selects the one which preserves the particle-hole symmetry of the model³⁰. Any other choice for the equation fixing the parameter p leads to a violation of the symmetry.

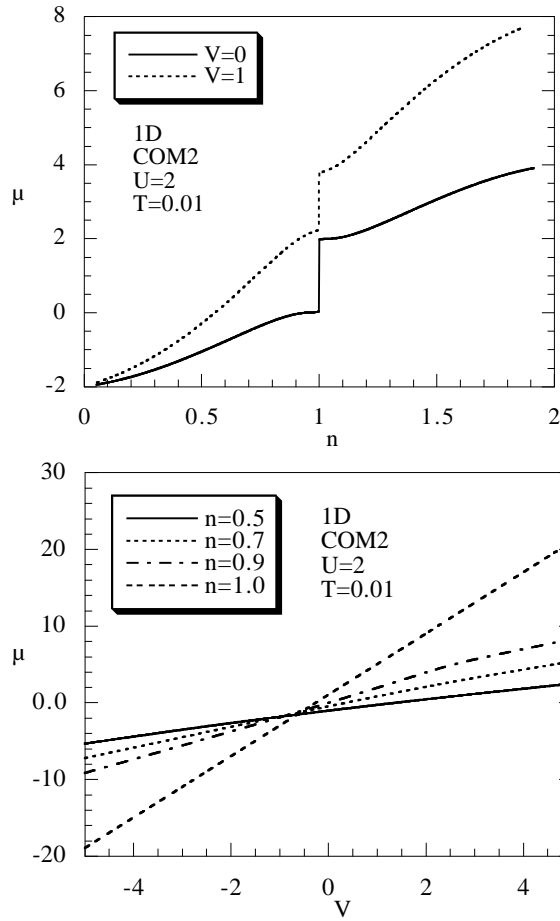


FIG. 1: The chemical potential at $U = 2$ as a function of: (top) the particle density for $V = 0, 1$; (bottom) the intersite Coulomb interaction for several values of n .

A. One-dimensional system

The chemical potential as a function of the particle density is reported in Fig. 1 (top) for $U = 2$ and $V = 0$ and 1. For any value of the filling the chemical potential increases by increasing the intersite Coulomb interaction and the increment is an increasing function of the filling: within the paramagnetic phase the average probability for two particles to be nearest neighbors increases with the filling and accordingly increases the free energy in the presence of a repulsive intersite Coulomb interaction, then, the behavior of the chemical potential follows.

For negative (i.e., attractive) values of the intersite Coulomb potential, we can see that the paramagnetic solution is unstable towards a phase with charge separation (i.e., with charge ordering). As a matter of fact, an attractive potential between charges at nearest neighbor sites favors a rearrangement of the particles in a one-particle-per-site scheme in order to maximize the gain in energy. At fillings less than one this scheme can lower the energy more and more by accepting more particle in the

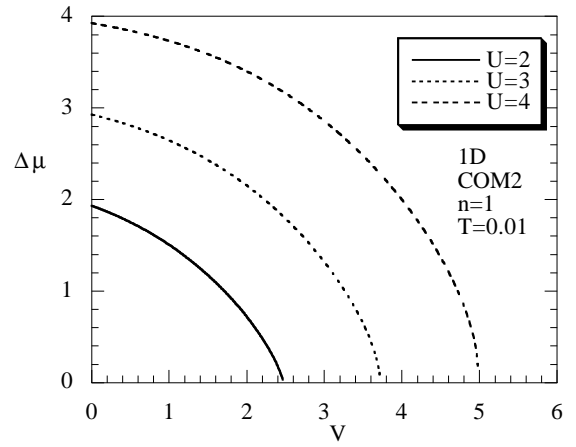


FIG. 2: The discontinuity of the chemical potential at half filling and $T = 0.01$ is plotted versus the intersite Coulomb interaction for $U = 2, 3$ and 4.

system and increasing the number of occupied couples of nearest neighbor sites. According to this, the chemical potential shows a negative slope which, on increasing the value of the intersite potential, manifests at lower and lower values of the filling. The critical value of the intersite Coulomb potential which controls the transition to the charge ordered state depends on the intensity of the local Coulomb interaction. In order to illustrate the case, in Fig. 1 (bottom), the chemical potential is given versus intersite Coulomb potential for $U = 2$ and various values of the particle density: all curves cross at a certain value $V \approx -0.5$, below which the system exhibits a negative compressibility.

As expected from the exact Bethe Ansatz solution of the one-dimensional simple Hubbard model, for any $U > 0$ there is a discontinuity at half filling, signalling a gap in the density of states and the occurrence of an insulating phase. As it can be seen from Fig. 1 (top), the effect of the intersite term V is to reduce the size of the gap. This is studied in Fig. 2 where the discontinuity of the chemical potential at half filling

$$\Delta\mu = \mu_+(1) - \mu_-(1) \quad (3.2)$$

is plotted versus the intersite Coulomb potential for various values of the onsite Coulomb potential at half filling and $T = 0.01$. We see that for a given value of the onsite Coulomb potential, there is a critical value V_c . For values of intersite Coulomb potential greater than V_c , the paramagnetic insulating phase becomes unstable (the chemical potential gets a negative slope) and there is a phase transition to a charge ordered insulating state (CO)²⁷. This kind of ordering is much different than that discussed previously (i.e., the one-particle-per-site type); in this case the repulsion among particles favors a checkerboard pattern with half sites double occupied (see in the next sections the discussion about the double occupancy) and half empty, these latter ones being the

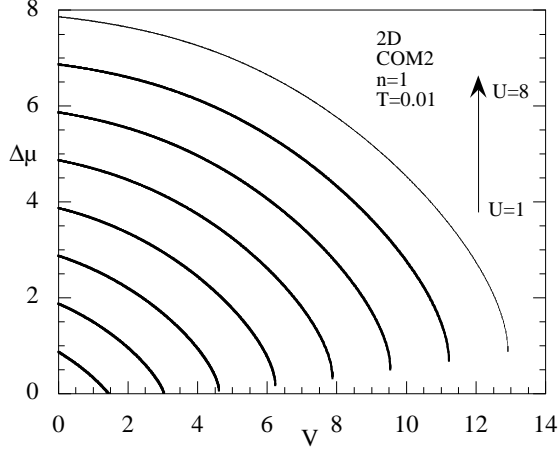


FIG. 3: The discontinuity of the chemical potential at half filling is plotted versus the intersite Coulomb interaction for various values of U and $T = 0.01$.

nearest neighbors of the former ones. By analyzing the derivative $[\partial(\Delta\mu)/\partial V]_{V=V_c}$, we can show that at zero temperature the transition is second order for $U \leq 2$ and first order for higher values of the onsite Coulomb potential.

B. Two-dimensional system

As already noted for the 1D system, also in 2D within COM2 solution the discontinuity $\Delta\mu$ of the chemical potential at half filling decreases by increasing the value of the intersite Coulomb potential and the system exhibits a phase transition to a charge ordered phase at some critical value V_c . The values of V_c , as a function of the onsite Coulomb potential, are shown in Fig. 3 where $\Delta\mu$ is reported versus the intersite Coulomb potential for various values of the onsite interaction U .

Within COM1 solution, the behavior of the chemical potential as a function of the particle density is shown in Fig. 4 (top) for $U = 4$ and various values of the intersite Coulomb potential. We see that for attractive values of the intersite Coulomb interaction the chemical potential decreases by increasing the filling, showing an instability of the paramagnetic case towards phase separation. In particular, exactly at quarter filling ($n=0.5$), we can have a charge-ordered state of one-particle-per-site type. Away from quarter filling, the phase separation is between two phases with different particle densities (these latter should be determined through a Maxwell construction), whose nature could be investigated (they can be both charge-disordered or one ordered and another disordered) within a treatment where translational invariance should be relaxed. The instability of the paramagnetic phase can be here studied by plotting the chemical potential as a function of the intersite Coulomb potential. This is shown in Fig. 4 (bottom) where we see that the

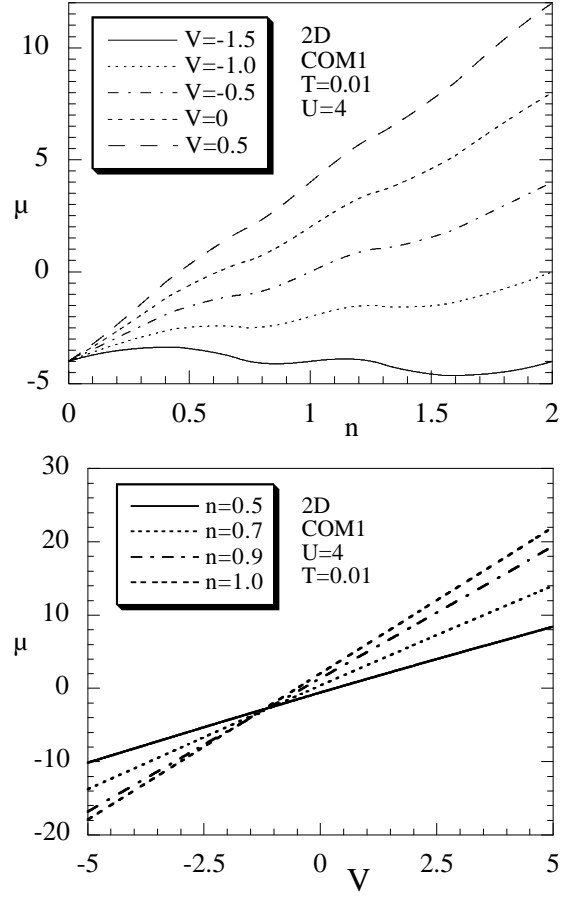


FIG. 4: The chemical potential at $T = 0.01$ and $U = 4$ versus: (top) the particle density for several values of V ; (bottom) the intersite interaction for several values of n .

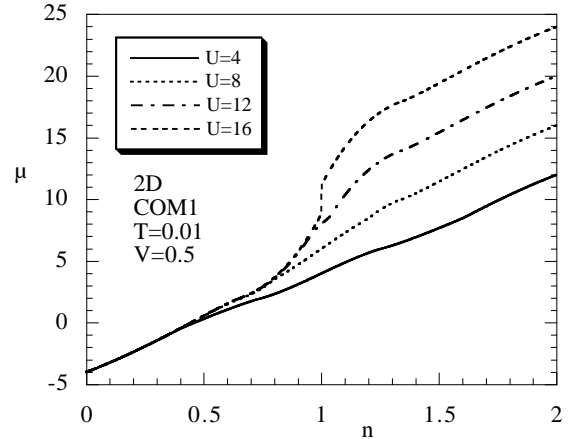


FIG. 5: The chemical potential versus the particle density at $T = 0.01$, $V = 0.5$ and several values of U .

curves for different values of filling all cross at some critical value V^* , depending on the onsite Coulomb potential [$V^* \approx -1.1$ for $U = 4$]. For $|V| < |V^*|$ the chemical potential is a decreasing function of the filling.

As in the simple Hubbard model^{45,50,51,52,53,54}, COM1 solution describes a metallic phase in the low regime of on-site Coulomb repulsion and a transition to the insulating state when the potential reaches some critical value. This feature survives also when the intersite Coulomb interaction is taken into account. For a fixed value of this latter, there is a critical value of the on-site repulsion such that the chemical potential exhibits a discontinuity at half filling. This latter signals the opening of a gap in the density of states and therefore a Mott transition. This feature is illustrated in Fig. 5. Now, the current study shows that the critical value U_c decreases by increasing the intersite potential V . By further increasing the intersite potential, the system undergoes a second transition to a charge ordered state of checkerboard type. This transition is characterized by a discontinuity in the double occupancy as commented above and shown in the next sections.

IV. PHASE DIAGRAMS

A. One-dimensional system

As reported in the previous section, COM2 solution for the one dimensional system shows that there is phase transition from the Mott insulating phase to a inhomogeneous charge ordered state of checkerboard type for positive values of the intersite Coulomb potential greater than some V_c . This result is consistent with many other studies^{22,27,55,56,57,58,59,60}. The nature of this phase transition is not well understood yet and currently under intense investigation^{57,58,59,60,61}. The phase diagram in the plane V - U is shown in Fig. 6, where the critical value V_c of the intersite Coulomb potential is plotted as a function of the onsite potential U . The arrow indicates the point where the phase transition from second order changes to first order.

It is necessary noticing that this transition is quite different from that usually observed in proximity of the $U = 2V$ line between an inhomogeneous charge ordered phase and an homogenous spin ordered phase. In this manuscript, we decided to focus on the homogenous paramagnetic phase, its instabilities towards charge ordered inhomogeneous phases (paying attention to the rank of the transition) and the relation between these latter and the metal-insulator transition. These kinds of transitions are the only ones relevant at room temperatures and/or in presence of frustration as the antiferromagnetic phase is quite depressed in such cases.

In Fig. 7 we give the phase diagram in the plane T - V for $U = 2$ and $U = 8$. For $U = 2$ the transition is second order for all values of T . For $U = 8$ the transition is first order for $T \leq 0.55$ and second order for

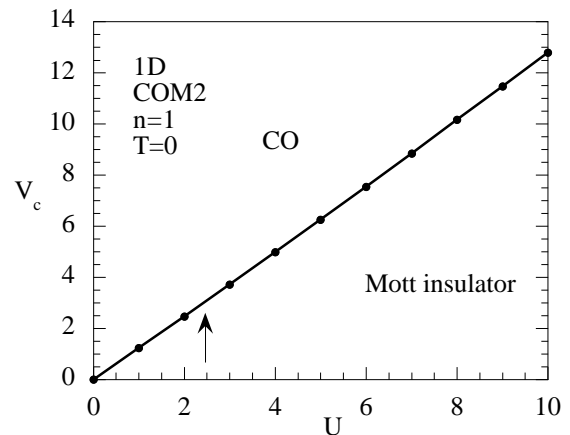


FIG. 6: The critical value V_c where there is a phase transition from the Mott insulator to charge ordered state is plotted as a function of the onsite Coulomb potential at half filling and zero temperature.

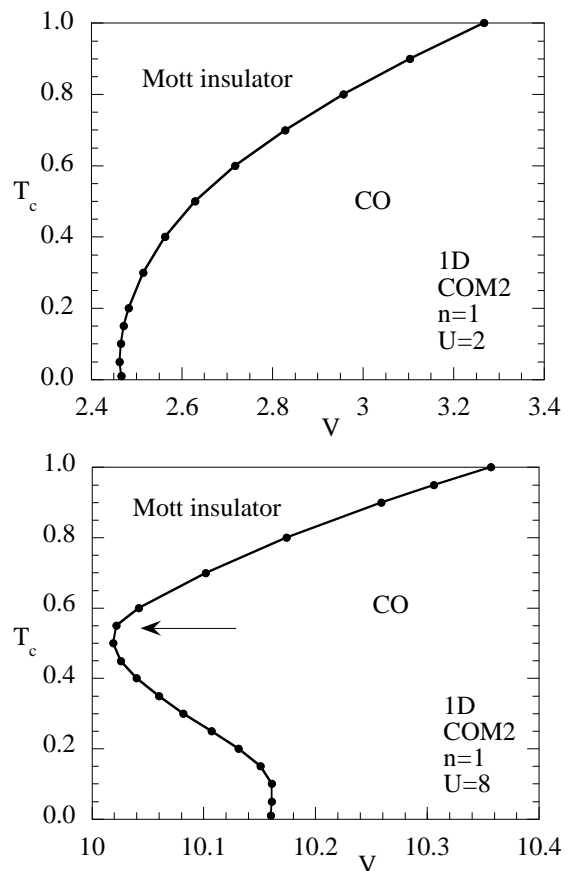


FIG. 7: The critical temperature T_c for the Mott insulator to charge ordered state phase transition is plotted as a function of the intersite Coulomb potential at half filling and $U = 2$ (top) and $U = 8$ (bottom).

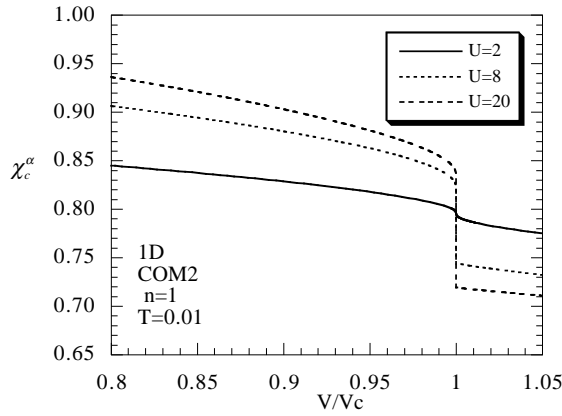


FIG. 8: The nearest-neighbor density-density correlation function χ_c^α is plotted as a function of V/V_c at half filling, $T = 0.01$ and $U = 2, 8$ and 20 .

$T \geq 0.6$. The arrow indicates the temperature where, by increasing T , the transition becomes continuous. It is interesting to observe that the transition is continuous if there is no reentrant temperature behavior. By this latter we mean a situation in which by increasing temperature we can first enter and then exit a phase when within another (e.g., see Fig. 7 (bottom) at $V = 10.1$ for increasing temperature from zero). When there is a reentrant temperature behavior, the transition is discontinuous up to the turning point, then becomes continuous. A reentrant temperature behavior has been experimentally observed^{32,33,34} and will be further discussed for the 2D system. It is worth noting that the transition is also marked by a discontinuity in the nearest-neighbor density-density correlation function $\chi_c^\alpha = \langle n^\alpha(i)n(i) \rangle$. This quantity is shown in Fig. 8 as a function of V/V_c at half filling, $T = 0.01$ and $U = 2, 8$ and 20 . At the transition χ_c^α is continuous for $U = 2$ and discontinuous for $U > 2$. The nearest-neighbor density-density correlation function is a decreasing function of the intersite potential as the repulsion diminishes the probability of finding neighboring sites occupied. In particular, at the transition this probability reduces with a change of concavity (second order transition) or with a discontinuity (first order transition).

B. Two-dimensional system: COM2

The COM2 solution for the two-dimensional case has similar characteristic to the 1D case. The phase diagrams in the planes $V-U$ and $T-V$ are shown in Figs. 9 (top) and 9 (bottom), respectively.

At zero temperature the transition is continuous for $U \leq 1.8$ and first order for $U > 1.9$. For finite temperature and $U = 8$ a reentrant behavior as function of temperature is observed. The transition is first order up to the turning point $T = 0.6$, then be-

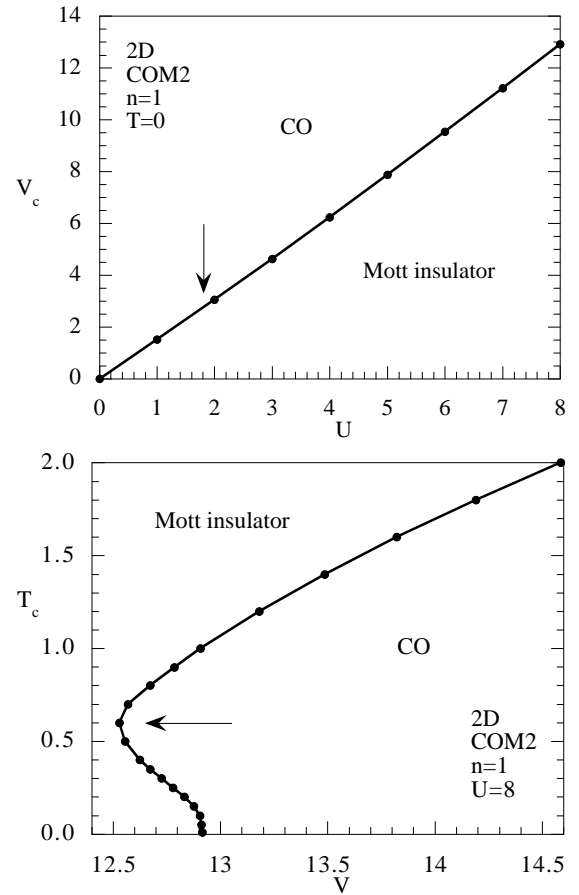


FIG. 9: (top) The critical value V_c for the Mott insulator to charge ordered state phase transition is plotted for the two-dimensional case (COM2 solution) as a function of: (top) the onsite Coulomb potential at half filling and zero temperature (COM2 solution); (bottom) V at half filling and $U = 8$.

comes continuous. For $U \leq 1.8$ no re-entrant behavior is observed. The fact that charge ordering may disappear by decreasing temperature has been experimentally observed in $Pr_{0.65}(Ca_{0.7}Sr_{0.3})_{0.35}MnO_3$ ³² and $La_{2-2x}Sr_{1+2x}Mn_2O_7$ ($0.47 \leq x \leq 0.62$)^{33,34}. On the theoretical side a re-entrant temperature has been obtained in the context of the extended Hubbard model at quarter filling^{23,26,28}.

In Fig. 10 (top) the nearest-neighbor density-density correlation function $\chi_c^\alpha = \langle n^\alpha(i)n(i) \rangle$ is plotted as a function of V/V_c at half filling, $U = 8$ and various temperatures. At the transition χ_c^α is discontinuous for $T = 0.01$ and $T = 0.4$, and continuous for $T = 1$, in agreement with the phase diagram shown in Fig. 9 (bottom).

C. Two-dimensional system: COM1

The results given for the chemical potential show that for low values of the on-site Coulomb interaction the sys-

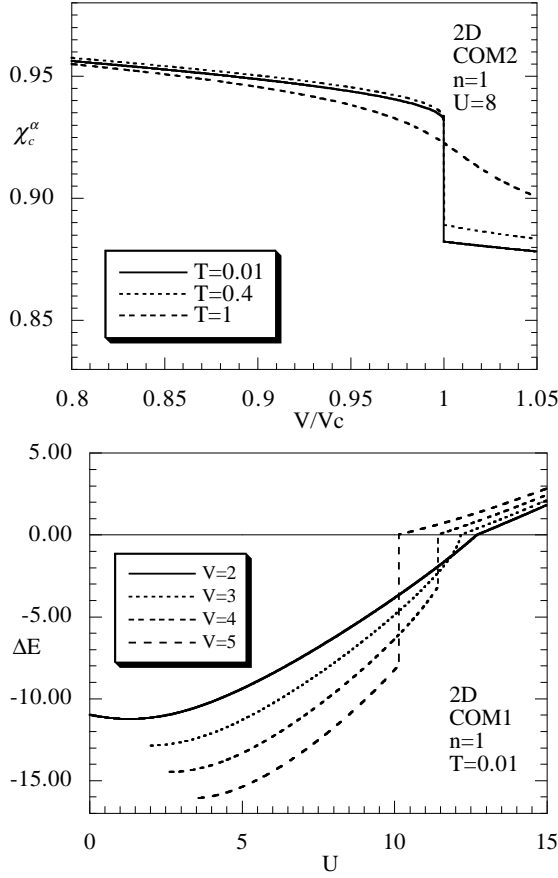


FIG. 10: (top) The nearest-neighbor density-density correlation function χ_c^α is plotted as a function of V/V_c at half filling, $U = 8$ and $T = 0.01, 0.4$ and $T = 1$, for the two-dimensional case (COM2 solution). (bottom) The energy gap ΔE at half filling is reported as a function of U for several values of U for $T=0$, for the two-dimensional case (COM1 solution).

tem is in a metallic state and undergoes a metal-insulator transition for a critical value U_c , which depends on the intensity of the intersite potential. In order to study this metal-insulator transition (MIT) we consider the quantity

$$\Delta E = E_1(0,0) - E_2(\pi,\pi) \quad (4.1)$$

which measures the distance between the bottom of the upper subbands and the top of the lower one. After Eq. (A4), at half filling we have

$$\begin{aligned} R(\mathbf{k}) &= R_1 \alpha(\mathbf{k}) & R_1 &= -8tp + 4V(C_{22}^\alpha + C_{11}^\alpha) \\ g(\mathbf{k}) &= g_0 & g_0 &= -U + 8V(1 - \chi_c^\alpha) \\ m_{12}(\mathbf{k}) &= m_1 \alpha(\mathbf{k}) & m_1 &= -4 \left[t \left(\frac{1}{2} - p \right) - VC_{12}^\alpha \right] \end{aligned} \quad (4.2)$$

Therefore, we simply have

$$\Delta E = 2R_1 + \sqrt{g_0^2 + 16m_1^2} \quad (4.3)$$

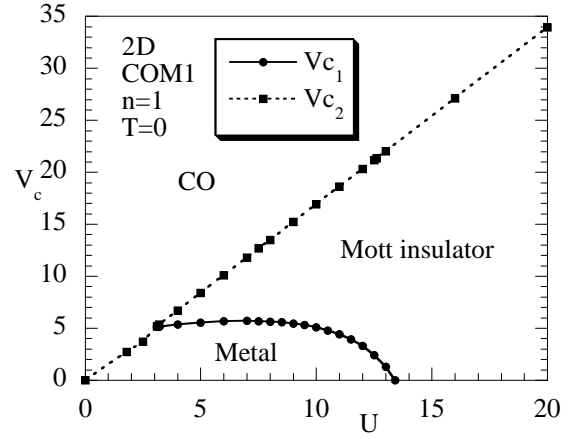


FIG. 11: The complete phase diagram in the plane U - V is shown at half filling for zero temperature, for the two-dimensional case (COM1 solution).

For a fixed value of the onsite Coulomb repulsion, the equation $\Delta E = 0$ will determine the critical value V_c where a metal-insulator transition occurs. The results show that the metallic region is compressed by the presence of the intersite interaction and disappears for $V > 5.7$. This is shown in Fig. 10 (bottom), where ΔE is reported versus the onsite Coulomb potential for various values of the intersite Coulomb potential at zero temperature.

For $V > 5.7$ the equation $\Delta E = 0$ does not have a solution and the metallic phase disappears. By further increasing the intersite Coulomb potential, there is an instability in the self-consistent equations (A9-A10), the double occupancy exhibits a discontinuity leading the system to a charge ordered state. The complete phase diagram in the plane V - U is shown in Fig. 11. The diagram is characterized by two critical values, V_{c1} and V_{c2} , which separate the different phases. V_{c1} controls the MIT and V_{c2} controls the transition to a charge ordered state. At V_{c1} the transition is first order for $U \leq 12$ and second order for $U \geq 12.2$; at V_{c2} we have first order for $U \geq 1.9$ and second order for $U \leq 1.8$. As proposed in Ref. 62, the insulating state can be characterized by the order parameters $\langle \xi_\sigma(j) \xi_\sigma^\dagger(j_{\text{odd}}) \rangle$ and $\langle \eta_\sigma(j) \eta_\sigma^\dagger(j_{\text{odd}}) \rangle$ which vanish at the MIT (j_{odd} is any site reachable in an odd number of hops from site j). The nearest neighbor hopping amplitudes $A = \langle \xi^\alpha(i) \xi^\dagger(i) \rangle = \langle \eta^\alpha(i) \eta^\dagger(i) \rangle$ and $B = \langle \eta^\alpha(i) \xi^\dagger(i) \rangle = \langle \xi^\alpha(i) \eta^\dagger(i) \rangle$ are reported in Figs. 12 as functions of the onsite Coulomb potential for various values of the intersite Coulomb potential. We see that for a given value of the intersite Coulomb potential, the probability amplitude A suddenly vanishes at some critical value of U_c and remains zero for all values of $U > U_c$. The probability amplitude B does not vanish above U_c . Owing to this contribution, we have that for $U > U_c$ the hopping of electrons from site j to a nearest neighbor is not forbidden, although restricted by the fact that

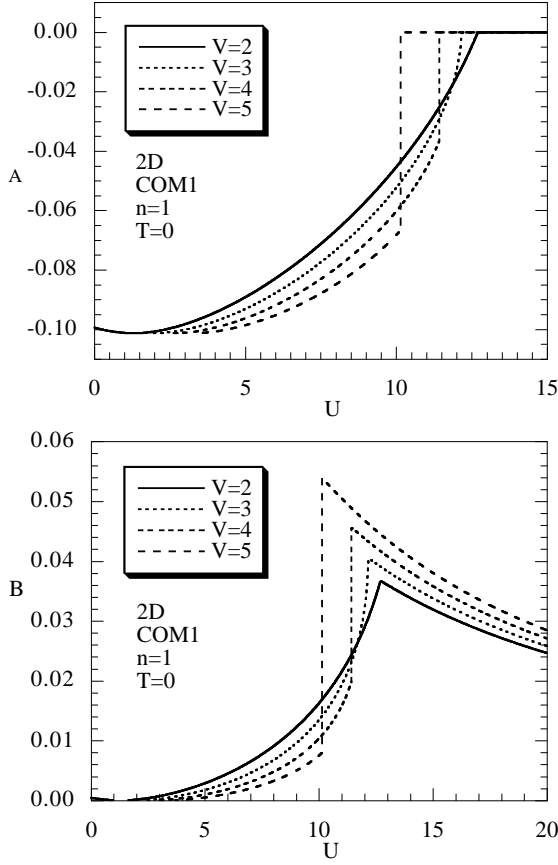


FIG. 12: The nearest neighbor hopping amplitudes A and B are reported as functions of the onsite Coulomb potential for various values of V , at half filling and $T = 0$.

$A = 0$. This is consistent with the fact that the double occupancy remains finite for $U > U_c$ and vanishes only in the limit $U \rightarrow \infty$ ⁶².

The phase diagram in the plane T - V is shown in Figs. 13 (top) and 13 (bottom). For $U = 15$ (see Fig. 13 (top)) there is no metallic phase and we have a critical temperature $T_c(V)$ where a transition from insulating to charge ordered state is observed. The transition is first order up to $T_c = 0.95$, then becomes continuous. A re-entrant temperature is observed with the same characteristics previously discussed. For $U = 8$ (see Fig. 13 (bottom)) we have two critical temperatures, T_{c1} and T_{c2} , which characterize the MIT transition and the insulator-charge order transition, respectively. Also in this case a re-entrant temperature is observed in the latter transition.

V. DOUBLE OCCUPANCY, KINETIC AND INTERNAL ENERGIES

In contrast to the local interaction U , a positive intersite interaction V favors the double occupancy $D =$

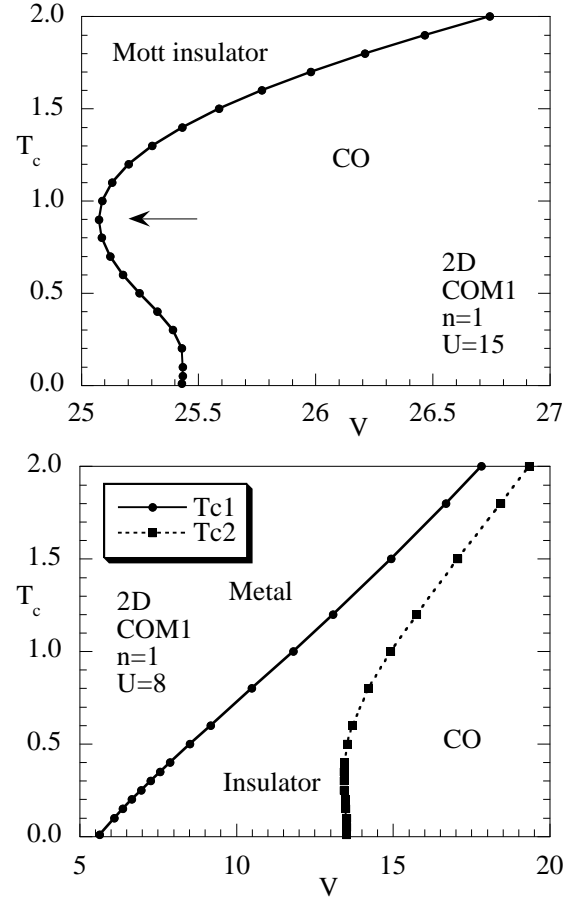


FIG. 13: The phase diagram in the plane $(V-T)$ is given for $U = 15$ (top) and $U = 8$ (bottom).

$\frac{1}{N} \sum_i \langle n_{\uparrow}(\mathbf{i}) n_{\downarrow}(\mathbf{i}) \rangle = \frac{n}{2} - C_{22}$. This happens through the mechanism which favors the formation of the checkerboard type charge ordered state as discussed above. The cost in energy U of having a double occupied site is partly balanced by the cost in energy V related to the presence of two particles on nearest-neighbor sites. On the contrary, an attractive intersite Coulomb interaction V leads to a decrement of the double occupancy as the one-particle-per-site type of charge ordering favors the presence of single occupied sites with respect to double occupied ones.

A. One-dimensional system

In Fig. 14 the double occupancy D is shown as a function of the particle density for $U = 2$ and several values of the intersite Coulomb potential up to the critical value V_c [for $U = 2$ we have $V_c \approx 2.47$]. The observed features agree with the expectation that the double occupancy increases with the intersite potential. At half filling the double occupancy exhibits a discontinuity at the critical value V_c [for $U = 4$ we have $V_c \approx 4.978$] (see Fig. 15).

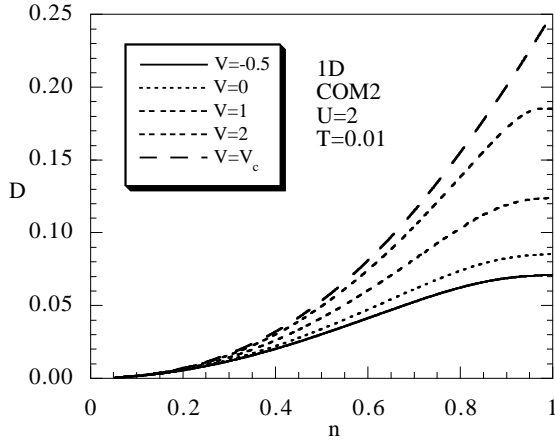


FIG. 14: The double occupancy versus the particle density at $T = 0.01$, $U = 2$ and several values of V .

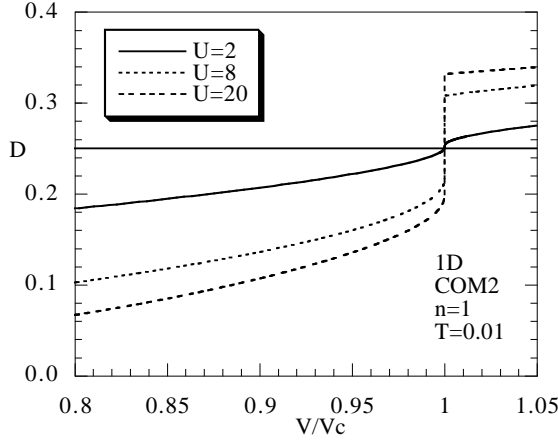


FIG. 15: The double occupancy at half filling versus V/V_c at $T = 0.01$ and several values of the onsite Coulomb potential.

Again, this is a signal of a phase transition from the Mott insulator to a CO state. It is interesting to observe that at the middle point of the jump, the double occupancy takes the value 0.25 (the noninteracting one) for all values of U . This result can also be inferred from Fig. 1 in Ref. 60. It seems as the effect of V completely neutralizes the effect of U and the system, at least for some local quantities, behaves as the noninteracting one.

From the Hamiltonian (2.1) we obtain the internal energy per site E_H

$$E_H = \frac{1}{N} \langle H \rangle = 4dt \langle c^\alpha(i) c^\dagger(i) \rangle + UD + dV \langle n^\alpha(i) n(i) \rangle \quad (5.1)$$

By increasing the intersite Coulomb potential the kinetic energy $K = 4dt \langle c^\alpha(i) c^\dagger(i) \rangle$ decreases and the internal energy E_H increases, respectively, owing to the fact that the double occupancy increases. This is shown in Fig. 16.

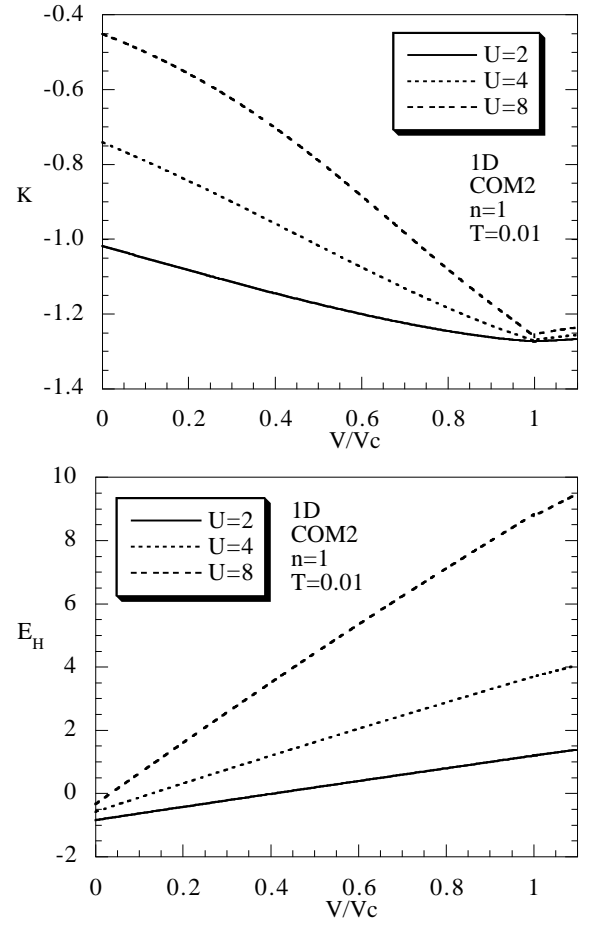


FIG. 16: The kinetic energy K and the internal energy E are plotted versus the intersite Coulomb potential, for $n = 1$, $T = 0.01$ and various values of the onsite Coulomb potential.

We can clearly see that the kinetic energy, as a function of the intersite Coulomb potential, shows a minimum at V_c when the transition is of the second order and develops a cusp when the transition is of the first order. The internal energy, instead, is almost insensible to the transition in the first case, but also develops a small cusp when the transition becomes of the first order (not shown).

B. Two-dimensional system

In Fig. 17, the double occupancy is plotted versus the filling for different values of the intersite Coulomb potential. The behavior is very similar to what has been found in the 1D case. On increasing the intersite Coulomb potential the double occupancy behaves as that of a noninteracting system (i.e., tends to $n^2/4$).

The double occupancy as a function of the onsite Coulomb potential is studied in Figs. 18 (top) and 18 (bottom). In Fig. 18 (top) we observe, by decreasing the onsite Coulomb potential, the transition from the insulat-

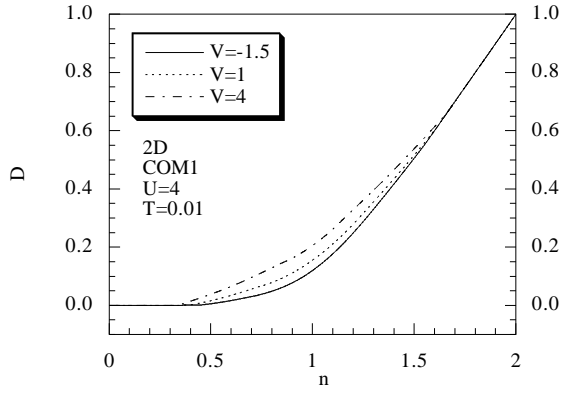


FIG. 17: The double occupancy versus the particle density at $T = 0.01$, $U = 4$ and several values of V .

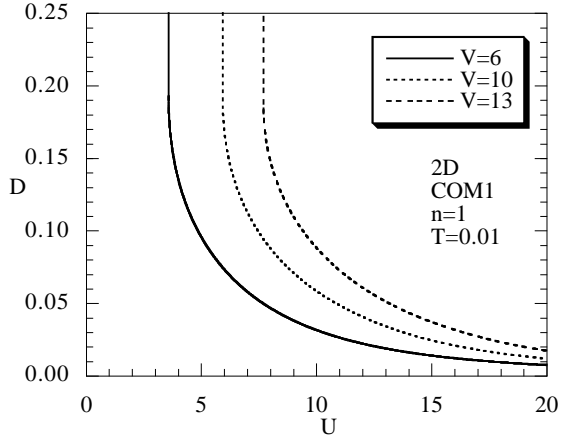
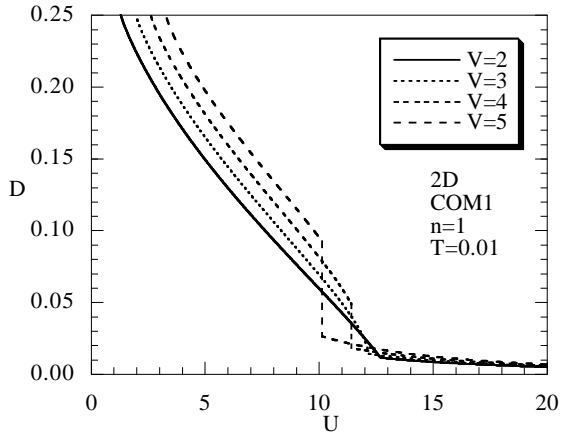


FIG. 18: The double occupancy versus the onsite potential at $T = 0.01$, half filling and several values of V .

ing phase to the metallic phase and to the charge ordered phase. In the insulating state the double occupancy is quite depressed; at the MIT there is a discontinuity and the double occupancy rapidly increases by decreasing the onsite Coulomb potential until encounters a second discontinuity when a CO phase comes into play. The case

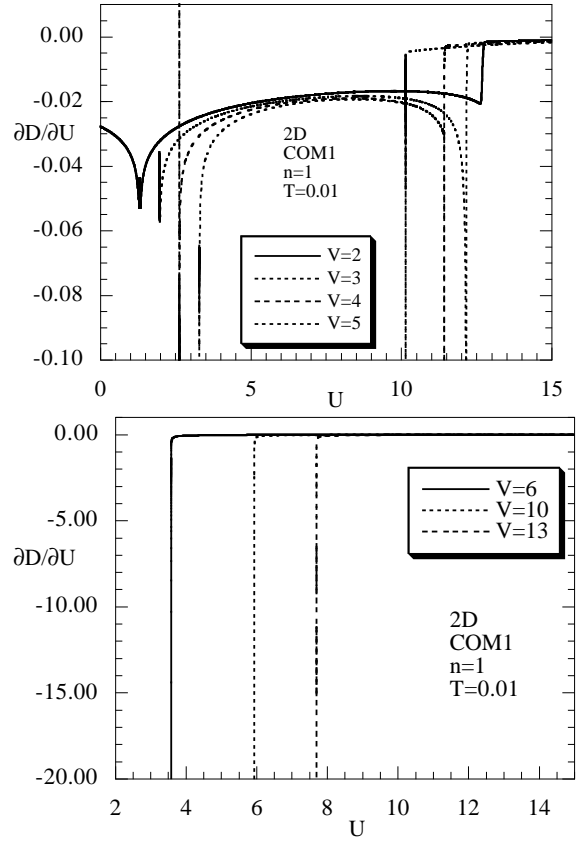


FIG. 19: The derivative of the double occupancy with respect to the onsite Coulomb potential is plotted versus the onsite potential at $T = 0.01$, half filling and several values of V .

where $V \geq 6$ is studied in Fig. 18 (bottom); in accordance with the phase diagram shown in Fig. 7, there is no metallic phase; by decreasing the onsite Coulomb potential, the double occupancy regularly increases until the charge ordered phase is reached.

The phase transitions are marked by a discontinuity in the double occupancy. This is shown in Fig. 19 where $(\partial D / \partial U)_{n=1}$ is plotted versus the onsite Coulomb potential for different values of the intersite Coulomb potential. For $V < 6$ (see Fig. 19 (top)) we have two discontinuities, related to the MIT and insulator to charge ordered phase transitions. For $V \geq 6$ (see Fig. 19 (bottom)) there is no metallic state and we observe only one discontinuity, related to the latter type of transition.

Accordingly to the behavior of the double occupancy, for positive values of the intersite Coulomb potential, the mobility of the electrons increases, signalling an overall tendency towards a charge density instability driven by the V term (see Fig. 20), in agreement with the mean-field result⁶³.

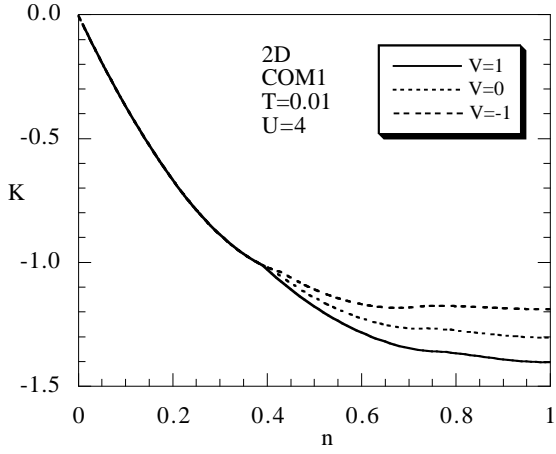


FIG. 20: The kinetic energy as a function of the particle density for $U = 4$, $T = 0.01$ and various values of V .

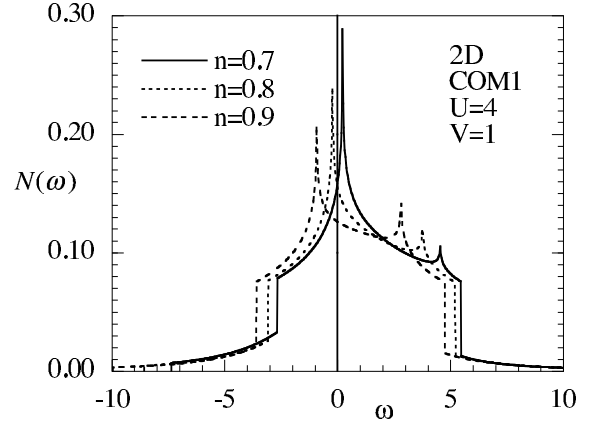


FIG. 22: The density of states at $U = 4$ and $n = 0.7, 0.9$ for $V = 1$.

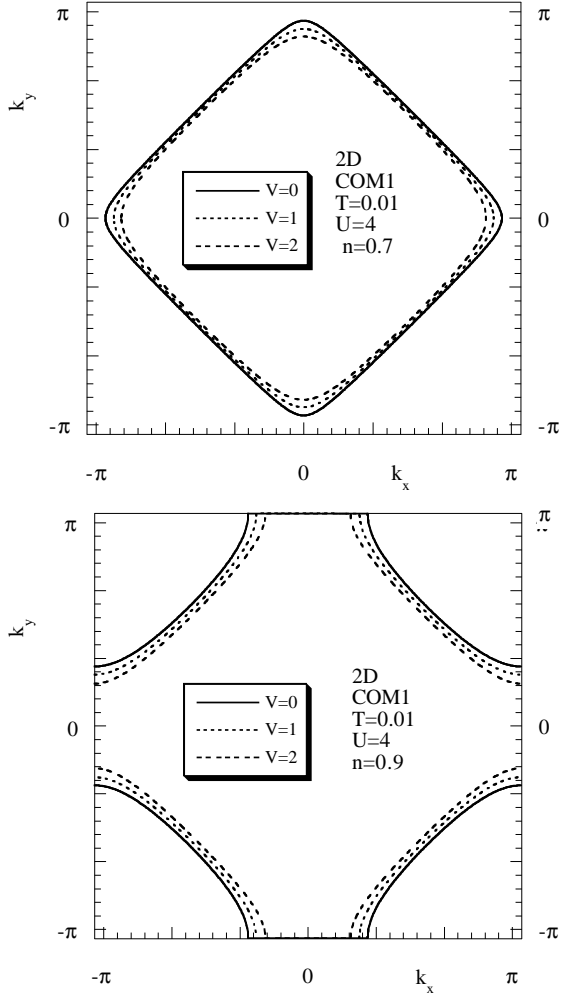


FIG. 21: The Fermi surface for various values of V at $U = 4$ and $n = 0.7, 0.9$.

VI. THE FERMI SURFACE AND THE DOS

With respect to what we have found in the simple Hubbard model⁶⁴, the overall shape and bending of the Fermi surface of the system does not change on varying the intersite Coulomb potential, but, almost rigidly, its volume decreases on increasing the intersite Coulomb potential [see Figs. 21]. This can be explained as an isotropic increment of the available states in \mathbf{k} -space and can be useful to describe quantitatively rather than qualitatively⁶⁴ (as the usual Hubbard model does) the ARPES determinations of the Fermi surface of the cuprate superconductors⁶⁵.

As we can see from Figs. 21 (top) and 21 (bottom), for given values of the onsite Coulomb potential and the intersite Coulomb potential, there is a critical value of the doping n_c where the Fermi surface is nested. At this critical value there is a crossing of the van Hove singularity and the Fermi level in the density of states (see Fig. 22).

This feature may be related, in the framework of the van Hove scenario, at the experimental results for the static susceptibility^{66,67} and specific heat^{68,69,70,71} in cuprate superconductors which exhibit well-defined peaks as functions of the filling. We have studied the value of the filling n_c , the result is shown in Fig. 23, where n_c is plotted as a function of the intersite Coulomb potential for various values of the onsite Coulomb potential. As we can see, n_c increases on increasing the intersite Coulomb potential until a certain value of $U \approx 8$ is reached. Above this critical value of the onsite Coulomb potential the influence of the intersite Coulomb potential is almost zero. This is a clear indication that if we would like to explain the cuprate superconductors and their anomalous features by means of Hubbard-like models, we need to exploit the intermediate regime for the onsite coupling and the weak regime for the intersite one. Only in this region of the model parameters, n_c is in qualitative

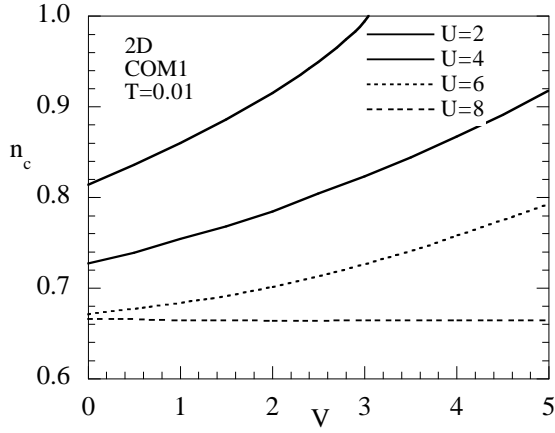


FIG. 23: The critical value n_c of the doping is shown as a function of V for various values of U .

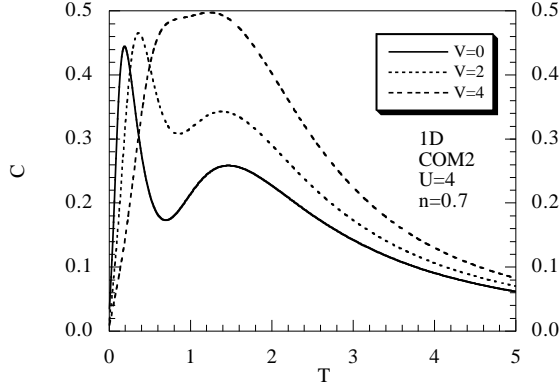


FIG. 24: The specific heat versus the temperature at $U = 4$, $n = 0.7$ and several values of V .

VII. THE SPECIFIC HEAT

The specific heat is shown in Fig. 24 for the one-dimensional case and in Fig.25 for the two-dimensional one.

A. One-dimensional case

In 1D, the net effect of the intersite Coulomb repulsion is to reduce the splitting between the charge and spin energy scales with respect to what observed for the simple Hubbard model, with a resulting more pronounced single peak at intermediate temperatures (see Fig.24).

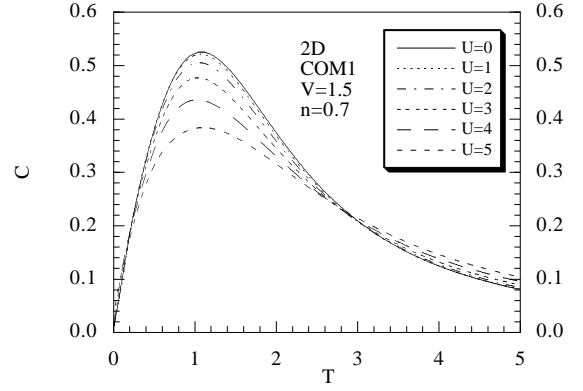


FIG. 25: The specific heat versus the temperature at $n = 0.7$, $V = 1.5$ and several values of U .

B. Two-dimensional case

As regards the 2D case, it is worth noting that there is a crossing point when the curves are plotted for different values of the onsite Coulomb potential at fixed V (see Fig.25), but there is no crossing point when the onsite Coulomb potential is fixed and different values of the intersite Coulomb potential are considered. This can be seen as an indication of the fact that the two interaction terms act to different orders in a perturbation expansion for the double occupancy and the kinetic energy. In particular, there is no value of temperature for which the first derivative of the double occupancy and the kinetic energy with respect to the intersite Coulomb potential does not depend on the intersite Coulomb potential.

VIII. CONCLUSIONS

The extended Hubbard model, in one and two dimensions, has been studied by means of the Composite Operator Method within the 2-pole approximation. According to the sign of the intersite Coulomb potential, transitions between the paramagnetic (metal and insulator) phase towards two kinds of charge ordered states (one-particle-per-site and checkerboard types) have been found. The rank of these transitions has been studied through the analysis of double occupancy, nearest-neighbor density-density correlator, kinetic and internal energies behavior. The evolution of the Fermi surface and of the nesting filling has been tracked on changing the value of the intersite potential evidencing the range of parameters suitable to describe the experimental features of the cuprate superconductors. The specific heat features on varying the intensity of the intersite potential has been contrasted to that found for the simple Hubbard model.

APPENDIX A: SPECTRAL DENSITY FUNCTIONS AND ENERGY SPECTRA

Within the 2-pole approximation, the energy spectra $E_i(\mathbf{k})$ and the spectral density functions $\sigma^{(i)}(\mathbf{k})$, appearing in Eq. 2.5, are given by

$$\begin{aligned} E_1(\mathbf{k}) &= R(\mathbf{k}) + Q(\mathbf{k}) \\ E_2(\mathbf{k}) &= R(\mathbf{k}) - Q(\mathbf{k}) \end{aligned} \quad (\text{A1})$$

$$\begin{aligned} \sigma_{11}^{(1)}(\mathbf{k}) &= \frac{I_{11}}{2} \left[1 + \frac{g(\mathbf{k})}{2Q(\mathbf{k})} \right] \\ \sigma_{11}^{(2)}(\mathbf{k}) &= \frac{I_{11}}{2} \left[1 - \frac{g(\mathbf{k})}{2Q(\mathbf{k})} \right] \\ \sigma_{12}^{(1)}(\mathbf{k}) &= \frac{m_{12}(\mathbf{k})}{2Q(\mathbf{k})} \end{aligned} \quad (\text{A2})$$

$$\begin{aligned} \sigma_{12}^{(2)}(\mathbf{k}) &= -\frac{m_{12}(\mathbf{k})}{2Q(\mathbf{k})} \\ \sigma_{22}^{(1)}(\mathbf{k}) &= \frac{I_{22}}{2} \left[1 - \frac{g(\mathbf{k})}{2Q(\mathbf{k})} \right] \\ \sigma_{22}^{(2)}(\mathbf{k}) &= \frac{I_{22}}{2} \left[1 + \frac{g(\mathbf{k})}{2Q(\mathbf{k})} \right] \end{aligned} \quad (\text{A3})$$

with the notation

$$\begin{aligned} R &= R_0 + R_1\alpha(\mathbf{k}) \\ R_0 &= -\mu + \frac{U}{2} + \frac{d}{I_{11}I_{22}} \left\{ -t\Delta + \frac{1}{2}V[n^2 + (1-n)\chi_c^\alpha] \right\} \\ R_1 &= \frac{d}{I_{11}I_{22}} \left\{ -t[p + I_{22}(1-n)] + V[I_{11}C_{22}^\alpha + I_{22}C_{11}^\alpha] \right\} \end{aligned} \quad (\text{A4})$$

$$\begin{aligned} g(\mathbf{k}) &= g_0 + g_1\alpha(\mathbf{k}) \\ g_0 &= -U + \frac{2d}{I_{11}I_{22}} \left[t(1-n)\Delta + \frac{1}{2}V(n^2 - \chi_c^\alpha) \right] \\ g_1 &= \frac{2d}{I_{11}I_{22}} \left[t(1-n)(p - I_{22}) + V(I_{22}C_{11}^\alpha - I_{11}C_{22}^\alpha) \right] \end{aligned} \quad (\text{A5})$$

$$\begin{aligned} m_{12}(\mathbf{k}) &= m_0 + m_1\alpha(\mathbf{k}) \\ m_0 &= 2dt\Delta \\ m_1 &= 2d[t(p - I_{22}) + VC_{12}^\alpha] \end{aligned} \quad (\text{A6})$$

$$Q(\mathbf{k}) = \frac{1}{2} \sqrt{g^2(\mathbf{k}) + \frac{4m_{12}^2(\mathbf{k})}{I_{11}I_{22}}}$$

$I_{11} = 1 - n/2$ and $I_{22} = n/2$ are the only non-zero entries of the normalization matrix; the parameters appearing in the previous equations are defined as

$$C_{\mu\nu}^\alpha = \langle \psi_\mu^\alpha(i) \psi_\nu^\dagger(i) \rangle \quad (\text{A7})$$

$$\begin{aligned} \Delta &= C_{11}^\alpha - C_{22}^\alpha \\ \chi_c^\alpha &= \langle n(i)n^\alpha(i) \rangle \\ p &= \frac{1}{4} \langle n_\mu^\alpha(i)n_\mu(i) \rangle - \langle [c_\uparrow(i)c_\downarrow(i)]^\alpha c_\downarrow^\dagger(i)c_\uparrow^\dagger(i) \rangle \end{aligned} \quad (\text{A8})$$

We can see that the Green's function depends on the following set of parameters: μ , C_{11}^α , C_{12}^α , C_{22}^α , p , χ_c^α . They can be computed as functions of the model parameters and temperature and filling by the following set of coupled self-consistent equations

$$\begin{aligned} n &= 2[1 - C_{11} - C_{22}] \\ C_{\mu\nu}^\alpha &= \langle \psi_\mu^\alpha(i) \psi_\nu^\dagger(i) \rangle \end{aligned} \quad (\text{A9})$$

$$\begin{aligned} C_{12} &= 0 \\ \chi_c^\alpha &= n^2 - \frac{n(2-n)}{n-2D} I_{11}^{-1} (C_{11}^\alpha + C_{12}^\alpha)^2 \\ &\quad - \frac{n(2-n)}{n-2D} I_{22}^{-1} (C_{12}^\alpha + C_{22}^\alpha)^2 \end{aligned} \quad (\text{A10})$$

where $C_{\mu\nu} = \langle \psi_\mu(i) \psi_\nu^\dagger(i) \rangle$ and $D = \frac{1}{N} \sum_{\mathbf{i}} \langle n_\uparrow(\mathbf{i}) n_\downarrow(\mathbf{i}) \rangle = \frac{n}{2} - C_{22}$ is the double occupancy.

The correlation function $C(i, j) = \langle \psi(i) \psi^\dagger(j) \rangle$ can be computed in terms of the retarded propagator, or better in terms of the energy spectra and of the spectral density functions, by means of the following expression³⁰

$$\begin{aligned} C(i, j) &= \frac{\Omega}{2(2\pi)^d} \sum_{n=1}^2 \int_{\Omega_B} d^d k e^{i[\mathbf{k} \cdot (\mathbf{i}-\mathbf{j}) - E_n(\mathbf{k})(t_i - t_j)]} \times \\ &\quad \times \sigma^{(n)}(\mathbf{k}) [1 + T_n(\mathbf{k})] \end{aligned} \quad (\text{A11})$$

where Ω and Ω_B are the volume of the unit cells in the direct and inverse spaces, respectively, and $T_n(\mathbf{k}) = \tanh(E_n(\mathbf{k})/2k_B T)$.

* E-mail: avella@sa.infn.it

† E-mail: mancini@sa.infn.it

¹ C. Varma, Sol. Stat. Comm. **62**, 681 (1987).

² P. Littlewood, C. Varma, and E. Abrahams,

- Phys. Rev. Lett. **63**, 2602 (1989).
- ³ C. Varma, Phys. Rev. Lett. **75**, 898 (1995).
 - ⁴ A. Janner, Phys. Rev. B **52**, 17158 (1995).
 - ⁵ J. van den Brink et al., Phys. Rev. Lett. **75**, 4658 (1995).
 - ⁶ J. Hubbard, Proc. Roy. Soc. A **276**, 238 (1963); **277**, 237 (1964); **281**, 401 (1964); **285**, 542 (1965).
 - ⁷ J. van den Brink, R. Eder, and G. Sawatzky, Europhys. Lett. **37**, 471 (1997).
 - ⁸ M. Simón, A. Aligia, and E. Gagliano, Phys. Rev. B **56**, 5637 (1997).
 - ⁹ J. Ferrer, M. Gonzáles-Alvarez, and J. Sanchez-Canizares, Phys. Rev. B **57**, 7470 (1998).
 - ¹⁰ E. Wigner, Trans. Faraday Soc. **34**, 678 (1938).
 - ¹¹ P. Fulde, Ann. Phys. **6**, 178 (1997).
 - ¹² E. Y. Andrei et al., Phys. Rev. Lett. **60**, 2765 (1988).
 - ¹³ A. Ochiai, T. Suzuki, and T. Kasuya, J. Phys. Soc. Jpn. **59**, 4129 (1990).
 - ¹⁴ C. H. Chen and S. W. Cheong, Phys. Rev. Lett. **76**, 4042 (1996).
 - ¹⁵ T. Ohama et al., Phys. Rev. B **59**, 3299 (1999).
 - ¹⁶ M. Vojta et al., Phys. Rev. B **62**, 6721 (2000).
 - ¹⁷ M. Salamon et al., Rev. Mod. Phys. **73**, 583 (2001).
 - ¹⁸ S. K. Park et al., Phys. Rev. B **58**, 3717 (1998).
 - ¹⁹ Y. Ueda et al., J. All. Comp. **317**, 109 (2001).
 - ²⁰ D. S. Chow et al., Phys. Rev. Lett. **85**, 1698 (2000).
 - ²¹ H. Seo and H. Fukuyama, J. Phys. Soc. Jpn. **67**, 2602 (1998).
 - ²² P. V. Dongen, Phys. Rev. B **50**, 14016 (1994).
 - ²³ R. Pietig, R. Bulla, and S. Blawid, Phys. Rev. Lett. **82**, 4046 (1999).
 - ²⁴ R. H. McKenzie et al., Phys. Rev. B **64**, 085109 (2001).
 - ²⁵ J. Merino and R. H. McKenzie, Phys. Rev. Lett. **87**, 237002 (2001).
 - ²⁶ A. Hoang and P. Thalmeier, J. Phys.: Condens. Matter **14**, 6639 (2002).
 - ²⁷ J. Hirsch, Phys. Rev. Lett. **53**, 2327 (1984).
 - ²⁸ C. Hellberg, J. Appl. Phys. **89**, 6627 (2001).
 - ²⁹ M. Calandra, J. Merino, and R. H. McKenzie, Phys. Rev. B **66**, 195102 (2002).
 - ³⁰ F. Mancini and A. Avella, Eur. Phys. J. B **36**, 37 (2003).
 - ³¹ F. Mancini and A. Avella (2004), preprint of the University of Salerno.
 - ³² Y. Tomioka et al., J. Phys. Soc. Jpn. **66**, 302 (1997).
 - ³³ T. Chatterji et al., Phys. Rev. B **61**, 570 (2000).
 - ³⁴ J. Dho et al., J. Phys.: Cond. Matt. **13**, 3655 (2001).
 - ³⁵ J. E. Hirsch and D. J. Scalapino, Phys. Rev. B **29**, 5554 (1984).
 - ³⁶ V. Emery, in *Highly Conducting One-Dimensional Solids*, edited by J. Devreese, R. Evrand, and V. van Doren (Plenum Press, New York, 1979), p. 247.
 - ³⁷ V. Emery, Phys. Rev. Lett. **58**, 2794 (1987).
 - ³⁸ F. Zhang and T. Rice, Phys. Rev. B **37**, 3759 (1988).
 - ³⁹ L. M. D. Bosch and L. Falicov, Phys. Rev. B **37**, 6073 (1988).
 - ⁴⁰ Y. Zhang and J. Callaway, Phys. Rev. B **39**, 9397 (1989).
 - ⁴¹ X.-Z. Yan, Phys. Rev. B **48**, 7140 (1993).
 - ⁴² A. Avella, S. Krivenko, F. Mancini, and N. Plakida, J. Magn. Magn. Mat. **272**, 456 (2004).
 - ⁴³ H. Matsumoto, T. Saikawa, and F. Mancini, Phys. Rev. B **54**, 14445 (1996).
 - ⁴⁴ H. Matsumoto and F. Mancini, Phys. Rev. B **55**, 2095 (1997).
 - ⁴⁵ F. Mancini, S. Marra, and H. Matsumoto, Physica C **252**, 361 (1995).
 - ⁴⁶ A. Avella, F. Mancini, M. Sánchez-Lopez, D. Villani, and F. D. Buzatu, J. Phys. Studies **2**, 228 (1998).
 - ⁴⁷ M. Sánchez-Lopez, A. Avella, and F. Mancini, Europhys. Lett. **44**, 328 (1998).
 - ⁴⁸ M. Sánchez-Lopez, A. Avella, and F. Mancini, Physica B **259**, 753 (1999).
 - ⁴⁹ A. Avella, F. Mancini, and M. Sánchez-Lopez, Eur. Phys. J. B **29**, 399 (2002).
 - ⁵⁰ F. Mancini, S. Marra, and H. Matsumoto, Physica C **244**, 49 (1995).
 - ⁵¹ F. Mancini, S. Marra, and H. Matsumoto, Physica C **250**, 184 (1995).
 - ⁵² A. Avella, F. Mancini, D. Villani, L. Siurakshina, and V. Y. Yushankhai, Int. J. Mod. Phys. B **12**, 81 (1998).
 - ⁵³ A. Avella, F. Mancini, and M. Sánchez-Lopez, J. Phys. Studies **2**, 232 (1998).
 - ⁵⁴ F. Mancini, H. Matsumoto, and D. Villani, J. Phys. Studies **3**, 474 (1999).
 - ⁵⁵ J. Cannon, R. Scalettar, and E. Fradkin, Phys. Rev. B **44**, 5995 (1991).
 - ⁵⁶ G. Japaridze and A. Kampf, Phys. Rev. B **59**, 12822 (1999).
 - ⁵⁷ M. Nakamura, Phys. Rev. B **61**, 16377 (2000).
 - ⁵⁸ M. Tsuchiizu and A. Furusaki, Phys. Rev. Lett. **88**, 056402 (2002).
 - ⁵⁹ P. Sengupta, A. Sandvik, and D. Campbell, Phys. Rev. B **65**, 155113 (2002).
 - ⁶⁰ E. Jeckelmann, Phys. Rev. Lett. **89**, 236401 (2002).
 - ⁶¹ M. Nakamura, J. Phys. Soc. Jpn. **68**, 3123 (1999).
 - ⁶² F. Mancini, Europhys. Lett. **50**, 229 (2000).
 - ⁶³ B. Chattopadhyay and D. Gaitonde, Phys. Rev. B **55**, 15364 (1997).
 - ⁶⁴ A. Avella, F. Mancini, and D. Villani, Sol. Stat. Comm. **108**, 723 (1998).
 - ⁶⁵ R. Markiewicz, J. Phys. Chem. Sol. **58**, 1179 (1997).
 - ⁶⁶ J. Torrance, A. Bezing, A. Nazzal, T. Huang, S. Parkin, D. Keane, S. LaPlaca, P. Horn, and G. Held, Phys. Rev. B **40**, 8872 (1989).
 - ⁶⁷ D. Johnston, Phys. Rev. Lett. **62**, 957 (1989).
 - ⁶⁸ J. Loram et al., Physica C **162**, 498 (1989).
 - ⁶⁹ N. Wada, T. Obana, Y. Nakamura, and K. Kumagai, Physica B **165-166**, 1341 (1990).
 - ⁷⁰ J.W. Loram et al., Phys. Rev. Lett. **71**, 1740 (1993).
 - ⁷¹ J. Loram et al., Physica C **235-240**, 134 (1994).